Severson, R. F., McDuffie, K. L.; Arrendale, R. F.; Chortyk, O. T. A Modified Method for the Rapid Analysis of Long Chain Alkanes and Neophytadiene from Tobacco. *Beitr. Tabakforsch. Int.* **1981**, *11*, 27–32.
Silverstein, R. M.; Bassler, G. C. *Spectrometric Identification of Organic Compounds*, 2nd ed.; Wiley: New York, 1976; pp 22–23.
Stoller, E. W.; Weber, E. J. Lipid Constituents of Some Common Weed Seeds. *J. Agric. Food Chem.* **1970**, *18*, 361–364.

Received for review November 1, 1988. Revised manuscript received March 31, 1989. Accepted April 26, 1989. Mention of a trademark, proprietary product, or vendor does not constitute a guarantee or warranty of the product by the U.S. Department of Agriculture and does not imply its approval to the exclusion of other products or vendors that may also be suitable.

Stability of Aqueous Foams: Analysis Using Magnetic Resonance Imaging

J. Bruce German* and Michael J. McCarthy

Aqueous foams differ widely in their structure and kinetic stability. Understanding and particularly assigning specific functional roles to individual components in the foams has been severely limited by the inability to analyze such unstable colloidal systems. We report the use of magnetic resonance imaging techniques in the description of foam structure and collapse. Foams from cream, egg white and beer were imaged, and the signal intensities contributed by aqueous protons were recorded sequentially over the lifetime of the foams. We were able to estimate densities, drainage rates, and collapse throughout the foam structure, noninvasively from actual food foams. This technique will be of use in the analysis of a variety of colloidal systems.

Foams are thermodynamically unstable colloidal systems in which gas is transiently maintained as a distinct dispersed phase in a liquid matrix (Adamson, 1982). These forms of matter are characterized by their low density, high viscosity and ultimately finite stability (Bikerman, 1973). There are a great many practical uses of aqueous foams in foods, pharmaceuticals, and engineering, and the number of novel applications is increasing rapidly (Aubert et al., 1986). Each foam system is unique in terms of its chemical composition and formation, and these differences lead to quite different macroscopic properties. For example, egg white protein stabilizes very high density foams in cakes, meringues, and candies (Cumper, 1953). Alternatively, novel surfactant solutions have proven to form effective very low density fire-fighting foams (Bikerman, 1973).

The formation, density, and ultimate stability of aqueous foams are critical parameters that must be characterized both in studying the basic mechanisms underlying foam chemistry and in practice estimating changes due to composition, i.e., food reformulation (Halling, 1981). Due to their inherent instability, sampling and measuring foams have proven very difficult (Halling, 1981; German et al., 1985). Model systems have been developed to examine foam collapse utilizing very precise measurements of pressure and conductance (Nishioka, 1986). These methods, though providing information for theoretical background, are not applicable to complex mixtures of surfactants and thus are inappropriate for studying most real foams. Noninvasive methods for describing foam development and collapse are critical to increasing our understanding of these events.

Magnetic resonance imaging (MRI) is a novel technology in which the strength of a signal associated with a resonant magnetic nucleus, i.e., proton ^1H, in a magnetic field can be assigned to a particular volume element in that magnetic field (Lauterbur, 1973). This allows one to generate images based not only on the presence of a nucleus in space but on its chemical structure and environment (Morris, 1986). The strength of MRI is that the image can provide density measurements as well as information on the local chemical environment (Morris, 1986). In addition to the spectacular breadth of chemical information available by this technique, it is also nondestructive and noninvasive. Sequential scans of materials can thus be used to follow changes in the chemical properties of matter dynamically. Foams are an intriguing model in which to apply this technology. In foam research one is interested in estimating densities and drainage rates without perturbing the structure of the foam to do it. MRI is uniquely suited to realize these goals. Our objective in this study was to employ MRI to monitor drainage from foams typical of food systems.

MATERIALS AND METHODS

Foams. Foams were generated with three well-known food systems: egg white, heavy cream, and beer. Egg whites were separated and 40-mL portions whipped for various times in a double-beater mixer (Sunbeam maximum speed). Typical final densities of the foams were approximately 0.15 g/mL. Heavy cream (40% fat) was chilled and again 40 mL whipped as above to densities of 0.3–0.4. Cylinders were punched from these foams using a Plexiglass chamber and immediately placed in the imaging coil of the NMR. For beer foams slightly different protocols were used. Commercial samples (30 mL) were carefully poured into a 100-mL glass beaker, and this was placed in an ultrasonic bath (Bransonic, Shelton, CN) and sonicated for 2 s. This effectively nucleated the dissolved CO_2 and generated approximately 50 mL of foam on top of 10–20 mL of liquid. Initial densities were therefore on the order of 0.3, although the very rapid drainage of these foams highlighted difficulties of the more traditional measurements of density. The glass beaker was then placed in the imaging coils.

Spectroscopy. A 2-T (General Electric, CSI) imaging spectrometer, with a 15-cm-i.d. imaging coil was used to measure ^1H signals at 85.5 MHz. A Fourier imaging spin-echo pulse sequence was used to generate the two-dimensional image. The same sequence with the pulse encode gradient turned off was used to

Department of Food Science and Technology, University of California, Davis, Davis, California 95617.

0021-8561/89/1437-1321$01.50/0

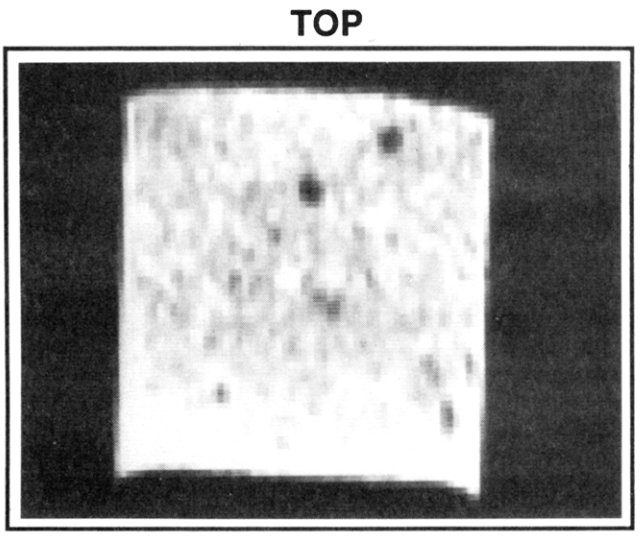

Figure 1. NMR image of whipped cream foam. Vertical 4-mm-thick planar image generated 10 min after formation of foam.

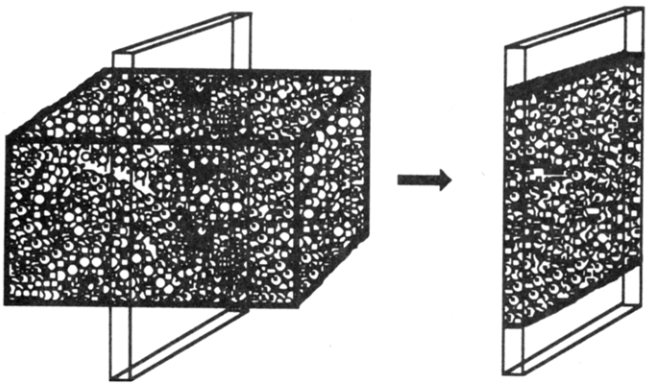

Figure 2. Schematic of a foam and the vertical 4-mm-thick plane imaged by the MRI system. The MRI system can be tuned to image on the basis of a variety of magnetic nuclei, and in this case the instrument was tuned to aqueous proton.

generate the one-dimensional spin projections. One acquisition was used for collecting data on beer; 16 acquisitions were used on the egg white foams and the whipped cream. Predelay values were set at 6 s for beer and 1 s for egg whites and whipped cream. Echo times were varied between 30 and 80 ms. T_1 values were determined from saturation recovery experiments, and T_2 values were estimated from Hahn spin-echo sequences modified with gradients to spatially encode the T_2.

RESULTS AND DISCUSSION

A two-dimensional image of an egg white foam is shown (Figure 1). The signal parameters of the instrument were tuned to protons primarily from water; hence, the image is essentially that of the continuous aqueous phase in the foam. At this resolution individual bubbles cannot be distinguished. However, with the proton signal associated with water, from the 4-mm-thick planar image in the vertical direction we obtain a signal whose strength is qualitatively proportional to the water content in the foam within that volume (Figure 2). We then generate a digitized intensity profile of the foam sample from top to bottom. The intensities corresponding to the foam image in Figure 1 are graphed in Figure 3. This proton signal profile is digitized and represents the analytical result used to develop estimates of density, drainage, and collapse.

The MRI signal is a function of nuclei density and the interactions of the nuclei with their local environment. This interaction is characterized by two relaxation time

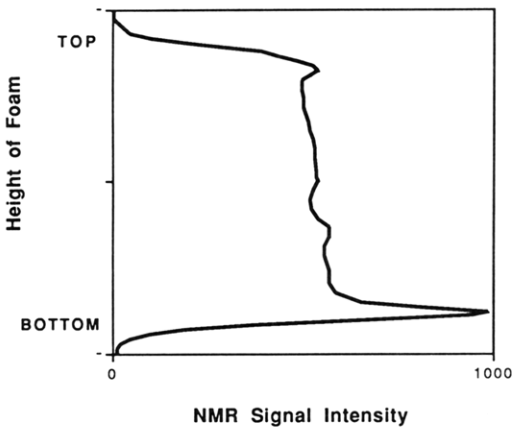

Figure 3. Signal intensity profile from foam in Figure 1. Digitized analysis generated a one-dimensional array of signal versus height of foam normalized to 100% for pure liquid at the bottom of the foam, uncorrected for relaxation effects.

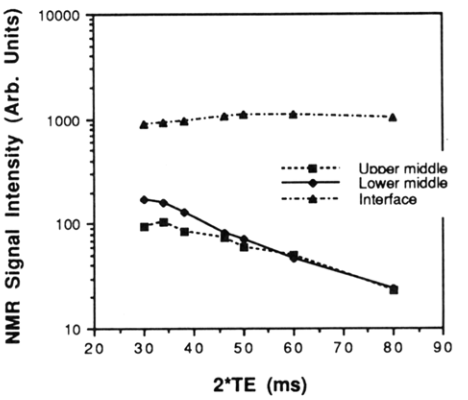

Figure 4. Variation in T_2 as a function of position within the foam. Values were calculated from signal intensities located at, respectively, the upper middle of the foam, lower middle of the foam, and the interface between foam and liquid.

constants: the spin–spin relaxation time constant (T_2) and the spin–lattice relaxation time constant (T_1). Signal intensity is directly related to nuclei density and an exponential function of the time constants as shown by

$$S \propto \rho \exp(-\mathrm{TE}/T_2)[1 - \exp(-\mathrm{PD}/T_1)] \qquad (1)$$

where ρ is density, TE is twice the delay time between the 90° and the 180° pulses, and PD is the predelay time between different signal acquisitions. Care must be taken to ensure that the influence of the time constants is accounted for when accurate values of density are desired. For instance, since the object being imaged is composed of foam and bulk liquid, we anticipate that the time constants will vary between the two parts of the sample and within the foam as a function of time. This requires that we measure the time constants as a function of position within the sample. Figure 4 shows the results for T_2 measurements at different positions within the foam. Note the dramatic difference in the shape of the spin-echo plot for different positions within the sample. Apparent T_2 values calculated for different positions in the egg white foam are approximately 50 ∓ 20 ms. However, it must be stressed that this is a rough estimate for the spin–spin relaxation time constant. Normally the spin–spin relaxation time constant is comprised of homogeneous and inhomogeneous contributions; additional components of the relaxation time constant in foams are the contributions due to drainage and collapse.

The drainage contribution can have either a positive or negative effect on the apparent spin–spin relaxation rate.

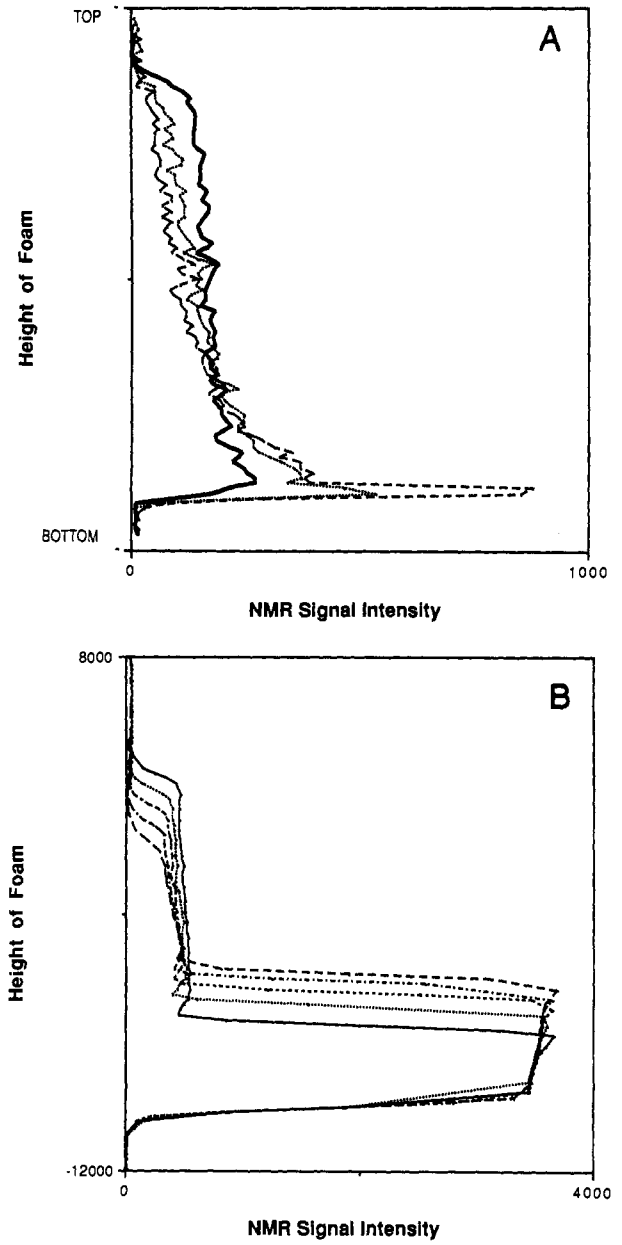

Figure 5. Sequential signal intensity profiles for egg white foam (A) and beer (B). Scans of egg white foam were taken at 2 (—), 6 (···), and 10 min (- - -) after formation. Scans of beer were taken at 30 (—), 60 (···), 90 (- - -), 120 (-·-), and 150 s (– –) after foam was generated with sonicator. Signal intensities plotted in these profiles are unadjusted for differences in relaxation rates.

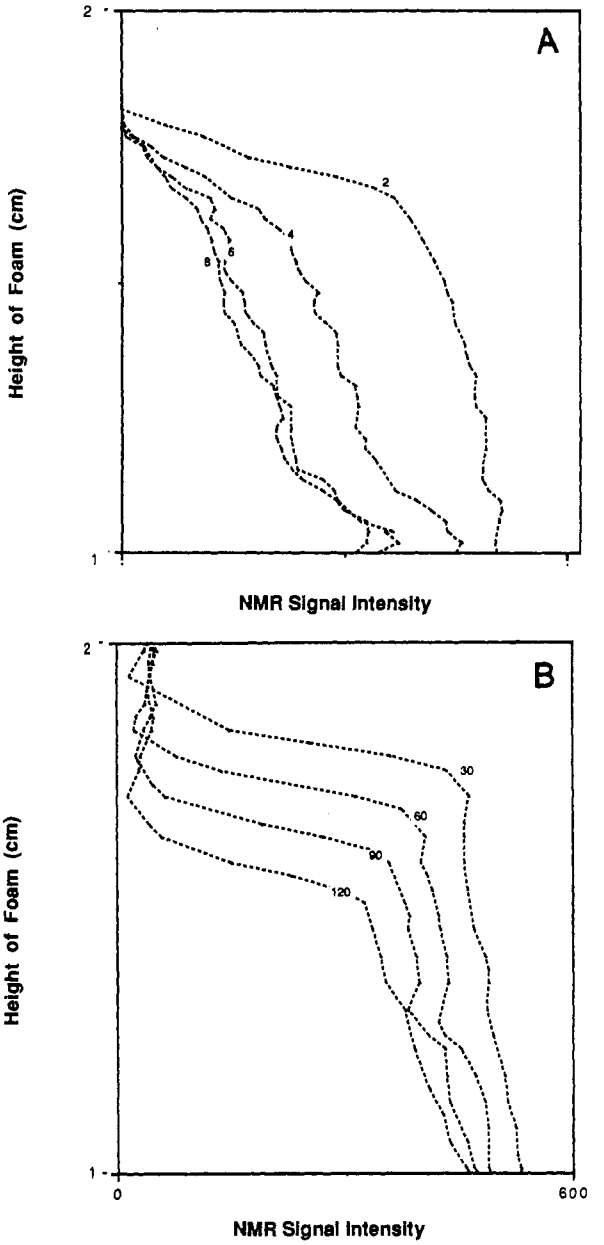

Figure 6. Scans of top of foam for egg white (A) and beer (B). Sequence times as shown on lines represent time after formation in minutes and seconds, respectively.

In the upper portions of the foam, fluid would be draining out of a volume element and hence would make the apparent T_2 smaller than the actual value. In regions of the foam close to the bulk liquid surface, liquid is most likely accumulating and would therefore make the apparent spin–spin relaxation rate appear larger than the actual value. In fact, the signal intensity, which should decrease as the TE is increased in a spin-echo experiment, can increase if enough liquid is flowing into the volume element. This increase is seen in Figure 4 for the region of the interface in an egg white foam.

Collapse of the foam would also have an impact on measurements of the spin–spin relaxation rate. Collapse in general should increase the local density of liquid and hence tend to increase the spin–spin relaxation time constant.

Once T_2 values are measured, the signal intensity profiles can be adjusted to correspond to the true vertical mass distribution. For example, the T_2 of egg white foam is 50 and is 300 ms for egg white liquid. Thus, by a spin–echo imaging sequence with a delay time set to 15 ms the signal intensity of the foam decayed by 25% and the signal intensity of the liquid by 5%. In addition to corrections for the spin–spin relaxation times, the differences in spin–lattice relaxation would also need to be used to correct the intensities.

Structure within a foam itself has been historically very difficult to measure, and hence estimates of density, drainage, and collapse have been limited to average density, overall volume, and fluid exiting the foam at the bottom. The MRI technique elegantly removes this limitation. In Figure 3, 10 min after foam formation, significant stratification of the foam is apparent from the asymmetry of the proton signal. The total water content (density) at the bottom of the foam column is significantly higher than at the top. With calibration of the proton signal and corrections for relaxation effects, actual densities can be determined. Thus, the ability of foaming methods to generate foams of a particular density can now be de-

termined in situ nondestructively.

The ability of the technique to rapidly accumulate sequential scans with time adds an even more important dimension. When the changes in proton signal across the imaging plane are followed with time, this measures the changes in density, hence a direct, noninvasive drainage pattern for every point in the foam. We are no longer limited to simply measuring liquid as it exudes from the bottom of the foam. MRI analysis can measure precisely the drainage rates throughout the foam.

This advance in technology has several immediate benefits. One of the important technical limitations in the measurements of foam breakdown until now is the inability to characterize the processes of drainage and bubble collapse independently. The ability of the imaging technique to distinguish distinct breakdown behaviors can be seen from analyses of two quite different foams: beer and egg white (Figure 5). Egg white is typically more stable than beer foam, and measurement rates were altered accordingly. In addition to the drainage rates, the drainage profiles are quite different. This is most clearly seen in an expanded view of the top of the foams (Figure 6). Liquid drains from the egg foam but maintains a finite bubble structure even to very low densities. Alternatively, the beer foam collapses completely as soon as the drainage reaches a critical liquid content. We interpret this as a reflection of the relatively poor ability of beer to form stable bubble films compared to the protein-stabilized films of egg white.

The MRI system has proven in initial studies to be extremely valuable in the description of the dynamic behavior of aqueous foams. Densities, drainage rates, and structural collapse can be readily calculated from digitized signal intensity profiles generated noninvasively from actual foods. The development of new velocity measurement pulse sequences such as spin-echo two-dimensional Fourier transform flow-compensated experiments should provide the techniques necessary to measure velocities within the foam (Majors et al., 1988). This combined with new developments, which may allow for collection of an entire image within several milliseconds (Mansfield, 1987), would allow for a complete understanding of both the structure and drainage of a foam. The breadth of physical and chemical information accessible to this technique suggests its use in the analysis of a variety of colloidal systems we are currently pursuing.

ACKNOWLEDGMENT

We thank J. R. Heil for recording the hydrogen spectra and transferring the data from the imaging spectrometer. We appreciate helpful discussions with Dr. Robert Kauten. This project was supported by a grant from the University of California, Davis, NMR Facility.

LITERATURE CITED

Adamson, A. *Physical Chemistry of Surfaces*, 4th ed.; Wiley: New York, 1982.

Aubert, J.; Kraynik, A.; Rand, P. Aqueous Foams. *Sci. Am.* **1986**, 74.

Bikerman, J. J. *Foams*; Springer-Verlag: New York, 1973.

Cumper, C. The stabilization of Foams by Proteins. *Trans. Faraday Soc.* **1953**, *49*, 1360.

German, J. B.; O'Neill, T. E.; Kinsella, J. E. Film forming and foaming behavior of food proteins. *J. Am. Oil Chem. Soc.* **1985**, *62*, 1358.

Halling, P. Protein stabilized foams and emulsions. *CRC Crit. Rev. Food Sci. Nutr.* **1981**, 155.

Lauterbur, P. C. Image formation by induced local interactions: Examples employing nuclear magnetic resonance. *Nature (London)* **1973**, *242*, 190.

Majors, P.; Altobelli, S.; Fukushima, E.; Givler, R. U.S. Department of Energy Contract Report SAND88-7011, 1988.

Mansfield, P. Rapid 3-D Magnetic Resonance Imaging. *J. Phys. C.* **1987**, *10*, L55.

Morris, P. G. *NMR Imaging in Medicine and Biology*; Clarendon Press: Oxford, 1986.

Nishioka, G. Stability of Mechanically Generated Foams. *Langmuir* **1986**, *2*, 649.

Received for review October 17, 1988. Revised manuscript received March 10, 1989. Accepted March 23, 1989.

Tannins in Wood: Comparison of Different Estimation Methods[1]

Augustin Scalbert,*[,2] Bernard Monties,[2] and Gérard Janin[3]

Different estimation methods of tannins—proanthocyanidins or hexahydroxydiphenoyl esters—have been compared and applied to polyphenols of various wood extracts. In the case of proanthocyanidins, reaction with vanillin in the presence of sulfuric acid is more sensitive than estimation by anthocyanidin formation. It is more specific than the assay by formaldehyde precipitation. Reaction with nitrous acid affords a selective estimation of hexahydroxydiphenoyl esters. These methods are applied to tannin estimation in wood extracts of 5 gymnosperms and 12 angiosperms and the values obtained compared to total phenols amounts.

Tannins are found in leaves, fruits, bark, and wood of most trees (Hillis, 1962; Scalbert et al., 1988). In woods such as quebracho (Hillis, 1962), they may account for over 20% of the dry matter. They are currently extracted from quebracho wood in South America and from chestnut wood in Europe and used in the leather industry.

Many of the tannin determination methods are based on their ability to form complexes with proteins (Deshpande et al., 1986; Hagerman, 1987). However, these methods do not take into account the structural heterogeneity of tannins. Indeed, tannins can be classified into two groups (Haslam, 1981): the proanthocyanidins (or condensed tannins) and the polyesters of gallic acid and (or) hexahydroxydiphenic acid (hydrolyzable tannins, re-

Laboratoire de Chimie Biologique (INRA), INA-PG, 78850 Thiverval-Grignon, France, and Station de Recherches sur la Qualité des Bois (INRA), CNRF, Champenoux, 54280 Seichamps, France.

[1] Presented in part at the 2nd Colloque Sciences et Industries du Bois, Nancy, April 22–24, 1987.

[2] INA-PG, Thiverval-Grignon.

[3] CNRF, Champenoux.

0021-8561/89/1437-1324$01.50/0